ORIGINAL RESEARCH

Production of cellulose nanofibrils from alfa fibers and its nanoreinforcement potential in polymer nanocomposites

Zineb Kassab · Assya Boujemaoui · Hicham Ben Youcef · Abdelghani Hajlane · Hassan Hannache · Mounir El Achaby

Abstract Alfa fibers (*Stipa Tenacissima*) were effectively utilized in this study as a promising cellulose source for isolation of carboxy-functionalized cellulose nanofibrils (CNFs) using multiple treatments. Pure cellulose microfibers (CMFs) were firstly extracted by alkali and bleaching treatments. CNFs with an average nanofibrils diameter ranging from 1.4 to 4.6 nm and a crystallinity of 89% were isolated from CMFs by a combination of TEMPO-oxidation and mechanical disintegration processes. The morphology and physico-chemical properties of cellulosic materials were evaluated at different stages of treatments using several characterization techniques. Various CNF loadings (5–15 wt%) were incorporated into PVA polymer to evaluate the nanoreinforcement ability of CNFs and to produce CNF-filled PVA nanocomposite materials. The tensile and optical transmittance properties, as well as the morphological and thermal properties of the as-produced CNF-filled PVA nanocomposite films were investigated. It was found that the tensile modulus and strength of nanocomposites were gradually increased with increasing of CNF loadings, with a maximum increase of 90% and 74% was observed for a PVA nanocomposite containing 15 wt% CNFs, respectively. The optical transmittance was reduced from 91% (at 650 nm) for neat PVA polymer to 88%, 82% and 76% for PVA nanocomposites containing 5, 10 and 15 wt% CNFs, respectively. It was also found that the glass transition temperature was gradually increased from 76 °C for neat PVA to 89 °C for PVA nanocomposite containing 15 wt%. This study demonstrates the importance of Alfa fibers as annual renewable lignocellulosic material to produce CNFs with good morphology and excellent properties. These newly developed carboxy-functionalized CNFs could be considered as a potential nanofiller candidate for the preparation of nanocomposite materials of high transparency and good mechanical properties.

Z. Kassab · H. Ben Youcef · A. Hajlane ·
H. Hannache · M. El Achaby (✉)
Materials Science and Nanoengineering Department
(MSN), Mohammed VI Polytechnic University (UM6P),
Lot 660 – Hay Moulay Rachid, 43150 Benguerir,
Morocco
e-mail: mounir.elachaby@um6p.ma

Z. Kassab · H. Hannache
Laboratoire d'Ingénierie et Matériaux (LIMAT), Faculté
des Sciences Ben M'sik, Université Hassan II de
Casablanca, B. P. 7955 Casablanca, Morocco

A. Boujemaoui
Wallenberg Wood Science Center, Department of Fiber
and Polymer Technology, KTH Royal Institute of
Technology, SE-10044 Stockholm, Sweden

Graphic abstract
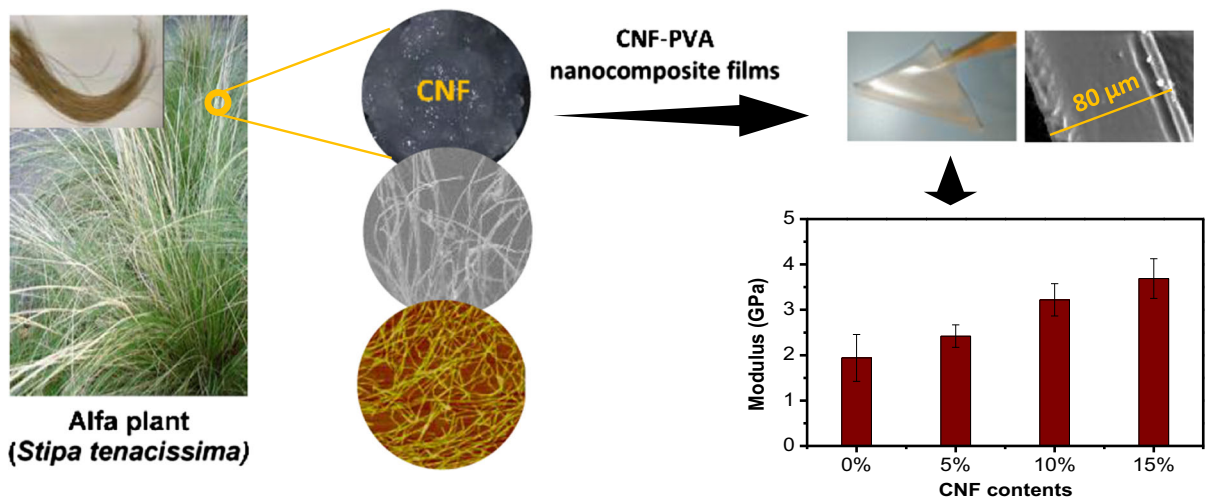
Keywords Alfa fibers · Cellulose nanofibrils · Polymer nanocomposites · Mechanical properties

Introduction

For several years, the emergence of concepts such as circular economy, sustainable development, industrial ecology and green chemistry are accompanied by the development of new generations of materials. Among these materials, fully biodegradable polymer composites are evolving into high-performance and low-cost products, while meeting environmental and regulatory requirements for recycling. Polymer-based nanocomposites reinforced with natural nanofillers are attracting more and more attention because of their ultimate properties that allow access to high value-added applications (Kılınç et al. 2018). Among the reinforcing nanofillers, nanocelluloses such as cellulose nanocrystals (CNCs) and cellulose nanofibrils (CNFs) have attracted significant interest in the last years. Renewability, sustainability and biocompatibility make cellulose-based nanofillers the candidate of choice for a wide range of applications (e.g., pharmaceutical, medical, paper manufacturing and packaging) (Trache et al. 2016a, 2017; Ferrer et al. 2017; Joy et al. 2017; Trache 2018; Goetz et al. 2018; Curvello et al. 2019; Jose et al. 2019).

Furthermore, the extraction process and the chemical/mechanical treatment of the cellulose are important for the end applications. In general, pure cellulose fibers (produced from lignocellulosic materials) can be chemically and/or mechanically disintegrated yielding nanosized cellulose namely CNCs and CNFs. CNC have high crystallinity with a diameter ranging from 5 to 25 nm and length less than 500 nm, while CNFs have relatively low crystallinity and have very small diameter (from 2 to 5 nm) and length of up to several microns (Thomas et al. 2018). CNFs attracted much attention compared to other biopolymeric nanomaterials, owing to their superior physicochemical properties, especially, the high aspect ratios (higher than 250), high elastic modulus (up to 145 GPa) and low thermal expansivity (2.7 ppm K^{-1}) (Koga et al. 2013; Gazzotti et al. 2019). The preparation of CNFs, from pure cellulose fibers, needs strong mechanical machining. However, chemical pretreatments such as TEMPO-oxidation process could be carried out before mechanical treatment. The TEMPO-mediated oxidation is used to selectively oxidize the primary alcohols on the surface of cellulose fibrils as pretreatment for improving fibrillation during the mechanical disintegration in water (Zhao et al. 2017).

The impact of CNF on physical and chemical properties of biodegradable polymer matrices such as Polylactic acid (PLA) and Polyvinyl alcohol (PVA) has been extensively studied for obtaining environmentally friendly nanocomposite materials (Wang et al. 2018; Gazzotti et al. 2019). Polyvinyl alcohol (PVA) is a biodegradable synthetic polymer with

excellent film-forming properties, flexibility, good chemical stability, non-toxicity and water-solubility (Liu et al. 2016; Poyraz et al. 2017; Singh et al. 2018). However, PVA films have comparatively poor mechanical properties and high-water vapor permeability, which can limit their use in several applications. Owing to the presence of hydroxyl groups (–OH) on its macromolecular chains, PVA can promote the formation of hydrogen bonds with CNF functional groups (Wang et al. 2018). Therefore, the incorporation of CNFs into the PVA matrix is suitable to achieve good mechanical and thermal properties without disturbing the transparency and biodegradability of PVA films (Singh et al. 2018). Besides, the reinforcement effect of the CNFs depends on several factors/parameters such as source of the raw materials, extraction process, and treatment type and conditions (Brinchi et al. 2013).

Although wood and cotton are the best-known resources for cellulosic fiber extraction, industries are steadily looking for alternative resources to meet their demand for cellulose-based materials. In this context, the identification of new resources abundant in nature, with favorable properties is highly relevant (Belouadah et al. 2015; Panyasiri et al. 2018). Various resources from field crops and agricultural residues such as rice straw, rice husk, sunflower stalks, alfa fibers, hemp fibres, sugarcane bagasse, palm tree rachis fibers, miscanthus fibers, bamboo pulp, spruce bark, sisal fibers, pineapple leaf fibers, garlic skin, soy hull, coconut husk fibres, mango seeds, red algae waste and banana peel waste are being increasingly employed for extracting cellulose-based materials and nanomaterials (Boufi et al. 2014; Collazo-Bigliardi et al. 2018; El Achaby et al. 2018a, b, d).

Alfa fibers, also known as *stipatenacissima* plant or *esparto*, are one of the most important bio-sourced materials for producing cellulose derivatives due to their high content of cellulose (44–48 wt%) and large availability (El Achaby et al. 2018d). In fact, this plant covers a large area in the North African countries, especially in Morocco (3,186,000 ha), Algeria (4,000,000 ha), Tunisia (400,000 ha) and Libya (350,000 ha) (El Achaby et al. 2018d). Alfa fibers were already identified as a viable and sustainable source for the production of microcrystalline cellulose (Trache et al. 2016b) and cellulose nanocrystals (El Achaby et al. 2018d) at relatively high yield and good quality.

In our recent work, CNC with high crystallinity and excellent thermal stability were extracted from Alfa fibers using sulfuric acid hydrolysis process and then used as nanoreinforcing agents to improve the tensile properties of various biopolymers including chitosan, alginate and carrageenan (El Achaby et al. 2018d). In this study, CNFs were extracted from raw Alfa fibers by alkali, bleaching and TEMPO oxidation treatments followed by mechanical disintegration process. The as-produced CNFs were successfully characterized using several techniques, namely atomic force microscopy, scanning electron microscopy, X-ray diffraction, thermogravimetric analysis and infrared spectroscopy. The as-extracted CNFs, at various weight loadings (from 0 to 15 wt%), were dispersed into PVA polymer matrix to produce CNF-filled PVA nanocomposite films using solvent casting method. The influence of CNF loadings on the properties of the resulting CNF-filled PVA nanocomposite films, including, morphology, transparency, thermal, and mechanical properties were extensively examined.

Materials and experimental details

Materials

The raw Alfa fibers (R-AF) used in this work were collected from the oriental region of eastern Morocco. The as-received R-AF (up to 100 cm fiber long and 2 mm in diameter) were cut into 1-2 cm long using a scissor. The PVA polymer (47,000 MW, 98.0–98.8 mol% hydrolysis) was purchased from Sigma-Aldrich and used as received. TEMPO, sodium bromide (NaBr), sodium chlorite (NaClO$_2$), glacial acetic acid solution, sodium hypochlorite solution (NaClO) and other chemicals were of laboratory grade (Sigma-Aldrich) and used as received without further purification.

Extraction of CNFs

Pretreatment

R-AF fibers were washed with distilled water for 1 h at 60 °C under mechanical stirring and then treated three times with 4 wt% NaOH solution at 80 °C for 2 h under stirring. The alkali-treated Alfa fibers (AT-AF) were bleached using a solution of equal parts (v:v) of

acetate buffer (pH 4.8) (27 g NaOH and 75 mL glacial acetic acid, diluted to 1 L of distilled water) and aqueous sodium chlorite (1.7 wt%). This treatment was performed for 2 h at 80 °C and repeated three times resulting in cellulose microfibers (CMFs), as confirmed by SEM observations. For all these treatments, fibers weight to liquid ratio was maintained to 1:20 (g:mL). For characterization, solid AT-AF and CMF materials were obtained by freeze-drying process. In this process, suspensions of AF–AF and CMFs were frozen using nitrogen liquid and then placed in a freeze-dryer (Cosmos-80, Cryotec) at − 60 °C for 48 h for complete removal of water. Finally, dry AT-AF and CMF powders were obtained. The final yield of the extracted CMFs was determined gravimetrically and found to be 40% with respect to the initial weight of R-AF.

The overall steps for AT-AF and CMFs extraction and digital images of the obtained products are illustrated in Fig. 1.

TEMPO-mediated oxidation of CMFs

20 g of the as-obtained CMFs were dispersed in 2 L of deionized water containing 2 g of NaBr and 12.5% NaClO solution (5 mmol/g). The pH of the mixture was adjusted to 10 by the addition of 0.1 M HCl solution. Then, 320 mg of TEMPO reagent was added to the mixture and the pH of the solution was maintained at 10 by adding 0.5 M NaOH solution. The TEMPO-oxidized CMFs (TO-CMFs) were thoroughly washed with deionized water and stored at

4 °C in wet form. A small amount of the obtained TO-CMF sample was freeze-dried for characterization using the same process described above. The carboxyl content of the TO-CMF sample was determined at 1640 µeq/g, as measured by conductometric titration according to the method of Saito et al. (2007). For that, 15 mL of 0.1 M HCl was added to 200 mL of TO-CMF aqueous solution (0.1 wt%), in order to completely neutralize the negative charges. After 10 min of stirring, the suspensions were titrated with the sequential addition of 0.01 M NaOH. The pH and the conductance were measured 1 min after each addition of NaOH. The conductometric titration was done three times, and the reported charge density is the average value.

Production of CNFs

CNFs were produced from the as-prepared TO-CMF via mechanical disintegration process. For that, 1 wt% TO-CMF aqueous suspension was subjected to mechanical treatment, which consisted in several passes through a microfluidizer M-110EH (maximum pressure 1600 bar, Microfluidics Ind., USA). Pair of 400 µm/200 µm chambers was used for the first pass at pressure ≤ 750 bar. Then two subsequent passes were carried out using 200 µm/100 µm chambers at pressure ≤ 1500 bar. This process resulted in the production of a transparent CNF gel with solid content of 1.38 wt% (Fig. 1). For CNF characterization, a small amount of the obtained gel was freeze-dried using the same process described above. The carboxyl content of the as-obtained CNFs was found to be similar to that measured for TO-CMF sample (1640 µeq/g), confirming the isolation of carboxy-functionalized CNF material.

Nanocomposites preparation

CNF-filled PVA nanocomposite films were prepared by solution casting technique. For that, 1 wt% PVA solution was obtained by dissolving PVA in distilled water under stirring for 1 h at 95 °C. The desired amount of CNFs was added to the PVA solution and the mixture was homogenized using an ultra-turrax mixer (IKA, D125 Basic, Germany) at 8000 rpm for 5 min. Subsequently, the PVA/CNF mixtures were cast onto rectangular plastic Petri dishes (120 × 120 mm²), and the water was evaporated at
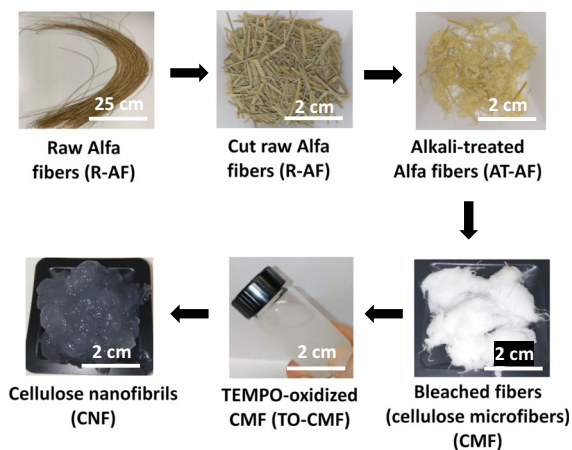

Fig. 1 Overall steps for CNF extraction and digital images of the obtained products at different stages of treatments

ambient temperature for 3 days. Neat PVA film was prepared following the same procedure without the addition of CNFs. The nanocomposite films were coded as PVA-CNF-X, where X indicates the weight loading of CNF (X = 5, 10 or 15 wt%). The thickness of nanocomposite films was measured using a hanatek variable force precision thickness gauge (FT3-V), which was determined as 77, 75, 80 and 78 μm for neat PVA, PVA-CNF-5, PVA-CNF-10 and PVA-CNF-15, respectively. It is worth noting that the thickness uniformity of films was controlled by the amount of the solution spilled into the Petri dishes (100 mL of each solution).

Characterization techniques

The morphology of the studied cellulosic materials and the cross-section of nanocomposite films were observed by scanning electron microscopy (SEM) using a Hitachi S-4800 apparatus operated at 15 kV. The nanocomposite films were frozen in liquid nitrogen and cryo-fractured for cross-sectional analysis. All samples were sputter-coated by a thin conductive carbon layer to help improve SEM observations.

Atomic force microscopy (AFM) images of CNFs were recorded using a Dimension ICON apparatus (Veeco, Bruker). Samples for AFM observations were prepared by depositing a droplet of a diluted CNF suspension (0.01 mg/mL) onto freshly cleaved mica sheets, after being sonicated for 5 min, and allowing the solvent to dry in air. The measurements were conducted in tapping mode under ambient temperature at a scan rate of 1.5 Hz and 512 scanning lines, using a cantilever with an 10 nm radius spherical tip (Silicon-tip on Nitride lever SNL-10, Veeco, Bruker). Scanning areas of 3.5×3.5 μm^2 and 1.5×1.5 μm^2 were analyzed. The obtained AFM images and the dimensions of CNFs were analyzed using Veeco data processing software (Nanoscope Version 8.0).

Fourier transform-infrared (FTIR) spectroscopy was performed on a Perkin-Elmer Spectrum 2000 FTIR apparatus equipped with attenuated total reflection (ATR) accessory. The FTIR spectra were recorded in 4000–600 cm^{-1} range with a resolution of 4 cm^{-1} and an accumulation of 16 scans.

X-Ray Diffraction (XRD) analysis was performed on a D2 PHASER diffractometer in Bragg–Brentano geometry (θ–θ). ACuKα radiation of wavelength of

1.5418 Å with a slit of 0.1 mm were used. During operation the electric voltage and current of the X-ray tube were 30 kV and 10 mA, respectively. The patterns were scanned through steps of 0.010142° (2θ), between 5 and 45° (2θ) with a fixed-time counting of 0.75 s/step. The crystallinity index (CrI) of different samples, was calculated using the following equation:

$$CrI = \frac{I_{200} - I_{am}}{I_{200}} \times 100$$

where I_{200} is the intensity of the (200) plane at around 2θ = 22.8°, and I_{am} is the intensity from the amorphous phase at approximately 2θ = 18.6° (French and Santiago Cintrón 2013; El Achaby et al. 2018a).

Thermal degradation behavior of all samples was performed using thermogravimetric analysis (TGA) (Discovery TGA, TA instruments). Samples of 5–8 mg were heated up from 25 to 700 °C under nitrogen atmosphere at a heating rate of 10 °C/min. The derivative thermogravimetric analysis (DTG), determined as the first derivative of the TGA analysis, was also measured for all studied samples to evaluate the rate of weight change. For neat PVA and its nanocomposites, the thermal parameters such as $T_{10\%}$ (the temperature corresponding to a weight loss of 10%), T_{max} (the maximum temperature in DTG curves) and the residual char values at 700 °C were measured to evaluate the thermal degradation behaviors of all polymeric films.

Glass transition temperature (T_g) of PVA nanocomposites was performed using differential scanning calorimetry (DSC) (Discovery DSC, TA instruments). Samples of about 5 mg were heated up from 25 to 150 °C under nitrogen atmosphere at a heating rate of 10 °C/min. The T_g value of each sample was determined from the obtained DSC curves by a data processing software (TRIOS, TA instruments) using the tangent method.

The UV–vis spectroscopy analysis of nanocomposite films was carried out using a Shimadzu UV-2550 UV–vis Spectrophotometer (Kyoto, Japan). The film samples with a rectangular shape (2×4 cm^2) were placed directly in the spectrophotometer test cell and the air was used as reference. The optical transmittance of the films was measured in the wavelength range of 200–800 nm.

Uniaxial tensile tests were carried out using a universal tensile testing system (Instron 5944, U.K.)

equipped with a 500 N load-cell and a video extensometer. Specimens of 5 mm wide and 80 μm thick were tested in quintuplicate. The gauge length was set at 20 mm and the cross-head displacement at 10%/min. The strain was also measured using the video extensometer that tracks two contrasting marks on the specimen. Before testing, all samples were preconditioned for 5 days at 23 ± 1 °C and 50% relative humidity.

Results and discussion

Extraction and characterization of CNFs

CNFs were successfully isolated from R-AF via chemical treatments followed by mechanical disintegration. The overall steps for CNF extraction are summarized in Fig. 1. R-AF were firstly treated by hot water (step not shown in Fig. 1) in order to clean and purify the fibers and to remove the hot water extractives (Trache et al. 2014). Once the dried R-AF were washed with hot water, they were subjected to an alkali-treatment to partially remove the non-cellulosic compounds such as lignin and hemicellulose molecules, resulting in yellow–brown AT-AF fibers (Fig. 1). These fibers have been partially dissociated due to the breaking of some alkali-labile bonds between lignin monomers or between lignin and polysaccharides (El Achaby et al. 2018c). The bleaching treatment was carried out to remove the residual lignin and hemicellulose molecules; in this process, AT-AF yellow–brown color which is most likely caused by phenolic compounds or lignin-based chromophores has been removed resulting in pure cellulose microfibers (CMFs) with clearly white color (Fig. 1) (Chen et al. 2017). The yield of CMFs was determined at 40% with respect to the initial weight of the starting R-AF. CNFs were prepared by TEMPO oxidation of CMFs (TO-CMFs) followed by progressive mechanical disintegration. For that, the TO-CMFs were subjected to mechanical treatment employing a microfluidizer at high pressure energy, resulting in a transparent CNF gel with a solid content of 1.38 wt% (Fig. 1).

Morphological analysis

The effect of the chemical and mechanical treatments on the morphology of the produced cellulosic fibers was evaluated by SEM and AFM observations, and the obtained results are illustrated in Fig. 2. Longitudinal SEM views of individual R-AF show that the outer surface of fibers presents small tips distributed in a regular and homogeneous way and surrounding the fiber bundle (Fig. 2a, b). These tips represent the comma-shaped cells found abundantly in the R-AF. Similar observations were reported in the literature for untreated R-AF (Mabrouk et al. 2012; Borchani et al. 2015). Generally, individual R-AF consists of several elementary fibers bonded together in the direction of their length by lignin and other non-cellulosic materials (Borchani et al. 2015). The comparison of different SEM micrographs of R-AF, AT-AF and CMFs shows clear morphological changes (Fig. 2a–d). The alkali-treatment resulted in partially defibrillated fibers (Fig. 2c), indicating the partial removal of non-cellulosic compounds (El Achaby et al. 2018d; Kassab et al. 2019b). The SEM micrograph obtained for CMFs (Fig. 2d) shows that the bleaching treatment resulted in the total defibrillation of fibers into individual microfibers with smaller diameter, which
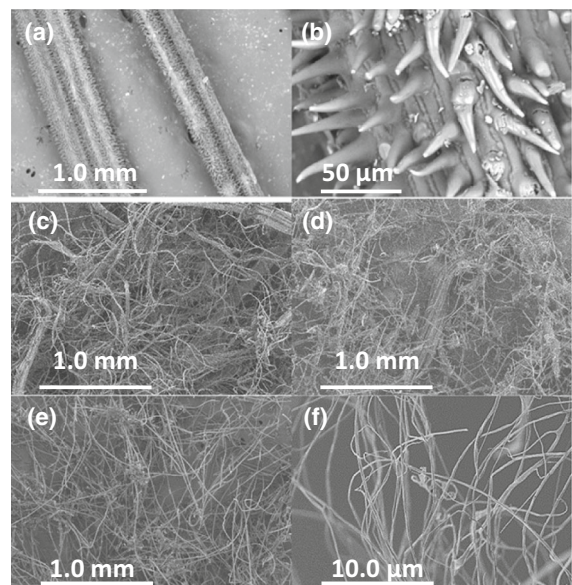

Fig. 2 SEM images of **a**, **b** R-AF, **c** AT-AF, **d** CMF, **e** TO-CMF and **f** CNF samples

can confirm the total removal of the no-cellulosic compounds.

TEMPO-mediated oxidation of CMFs (TO-CMFs) resulted in the total defibrillation of microfibers, as can be observed in Fig. 2e. Such oxidation can individualize microfibers by breaking hydrogen bonds between microfibers and inducing electrostatic repulsions, while the oxidized microfibers (TO-CMFs) retained the same macroscopic fiber and fragment morphologies with respect to unoxidized CMFs (Fig. 2d). The obtained SEM micrograph of the freeze-dried CNFs showed self-assembled nanofibrils with a diameter of hundreds of nanometers and length exceeding tens of micrometers (Fig. 2f). These dimensions suggest that the CNF associate with each other into superfine nanofibrils, due to the agglomeration phenomena resulted from the freeze-drying process.

AFM images (Fig. 3) confirmed the successful extraction of CNFs at nanometric scale in diameter. In fact, CNFs appear like aggregated bundles consisted of thin wire-like nanofibrils with a diameter of few nanometers. It was found that CNFs exhibited a widely distributed diameter, ranging from 1.4 up to 4.6 nm and length of more than a few microns. Indeed, the aggregation and entanglement of CNFs do not allow
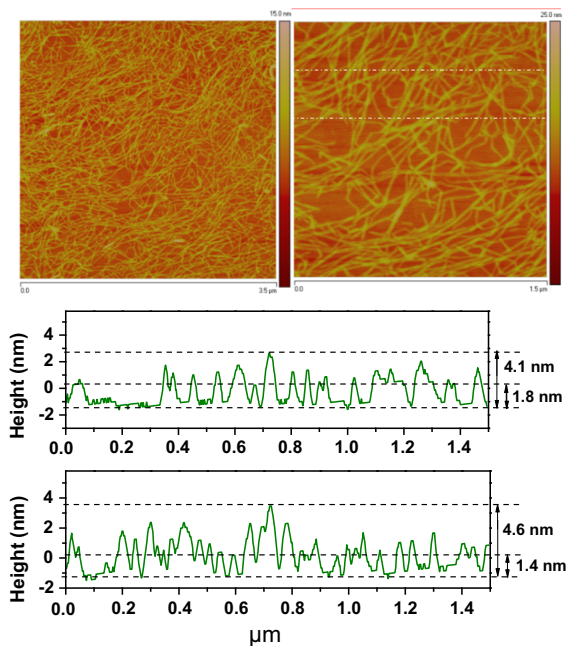

Fig. 3 High- and low-magnification AFM images of CNFs (top), and two representative height profiles taken along the indicated lines in AFM image

accurate determination of their lengths. Depending on the pretreatment involved, the dimensions of CNFs are usually between 3 and 20 nm in width, 500–2000 nm in length, and possess an aspect ratio greater than 250 (Koga et al. 2013; Dong et al. 2015). Herein, the observed narrow diameter (1.4–4.6 nm) of CNFs might be explained by the relatively high carboxyl content (1640 µeq/g) inTO-CMF material used for mechanical disintegration, which is higher than previously reported value (Wei et al. 2012).

Structural and thermal analysis of cellulosic materials

FTIR spectroscopic technique was applied to evaluate the chemical composition and the surface functionality of materials at different stages of treatments. Figure 4a illustrates the FTIR spectra of all studied materials. All the samples show the characteristic peaks of pure cellulose. The region between 3548 and 3039 cm^{-1} mainly originated from OH groups (Zhao et al. 2017), while the peaks at 2847–2910 cm^{-1} arise from the C–H symmetrical stretching (Zhao et al. 2017). The C–C and C–O skeletal vibrations gave prominent band at 1322 cm^{-1} (Kumar et al. 2014; Lam et al. 2017). At 1150 cm^{-1}, a peak arises from the C–O stretching vibration and anomeric carbon of b-D-glucopyranosyl of cellulose (Liu et al. 2013). Other peaks due to C–O–C glycosidic ether band and C–O–C pyranose ring skeletal vibration appear at 1099 cm^{-1} and 1031 cm^{-1} (Mandal and Chakrabarty 2011; Zhao et al. 2017). The peak at 895 cm^{-1} corresponded to the glycosidic –CH deformation with a ring vibration and –OH bending in β-glycosidic linkages between glucoses in cellulose. A band at 664 cm^{-1} is attributed to the out of plane deformation of C–H functional group (Zhao et al. 2017). R-AF sample is characterized by a peak at 1729 cm^{-1} attributed to the acetyl and uronic ester groups of hemicellulose or the ester linkage of carboxylic group of ferulic and *p*-coumaric acids of lignin and/or hemicelluloses (Trache et al. 2014; El Achaby et al. 2018d). The peaks at 1518 and 1235 cm^{-1} can be assigned to the C=C stretching vibrations from the aromatic ring and C–O out-of-plane stretching vibration of the aryl group in lignin and hemicellulose molecules (El Achaby et al. 2018d). Compared to R-AF spectrum, the peaks assigned to hemicellulose and lignin molecules disappeared in AT-AF and CMF spectra (Fig. 4a), confirming the effectiveness of the
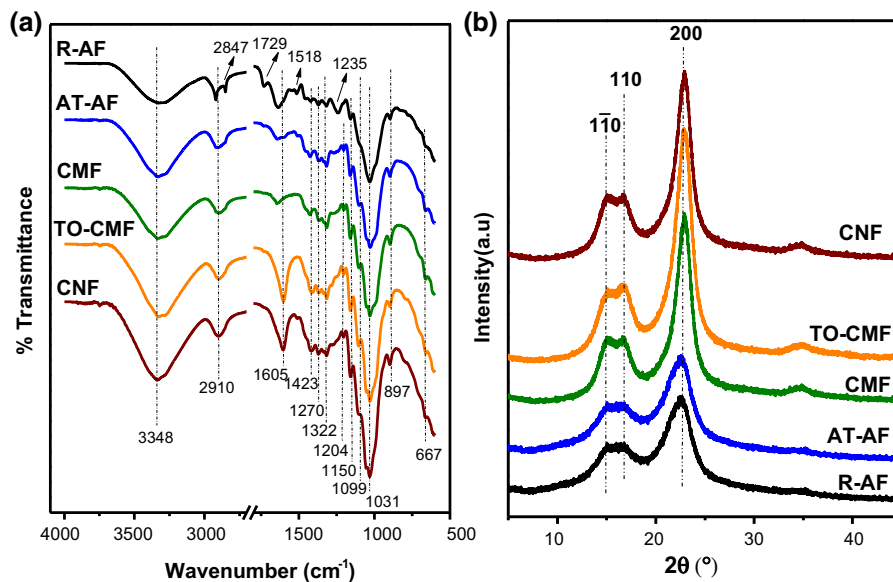
Fig. 4 a FT-IR spectra and **b** XRD patterns of R-AF, AT-AF, CMF, TO-CMF and CNF samples

alkali and the bleaching treatments for the removal of such non-cellulosic compounds (Trache et al. 2014; El Achaby et al. 2018d). The TO-CMF and CNF spectra show the two characteristic peaks at 1605 cm^{-1} and 1729 cm^{-1} representing COO$^-$ and COOH, respectively. Hence, confirming the partial oxidation of hydroxyl groups of native cellulose into carboxylic groups (Lasseuguette 2008; Wu et al. 2019b).

XRD diffractograms of R-AF, AT-AF, CMF, TO-CMF and CNF samples were recorded to evaluate the crystalline structure and the crystallinity index of each material. As illustrated in Fig. 4b, the XRD patterns displayed the typical signal of cellulose *I* structure, with strong crystalline peaks at 14.8, 16.8, and 22.9°, corresponding to $1\bar{1}0$, 110 and 200, crystal planes, respectively (French 2014). The crystallinity index (*CrI*) of R-AF, AT-AF, and CMFs is determined as 67%, 69% and 87%, respectively. This increase in *CrI* is due to the progressive removal of lignin and hemicelluloses during the alkali and bleaching treatments. A comparable *CrI* of about 88% is determined for the TO-CMFs, which might result from their natively highly ordered crystalline structure (Wei et al. 2012; Zhao et al. 2017). In fact, the introduction of carboxyl groups by TEMPO-mediated oxidation did not deteriorate the internal cellulose crystallites. After the mechanical disintegration, the resulted CNFs showed a *CrI* of 89%, which is comparable to that

measured for CMFs (87%) and TO-CMFs (88%). It is well known that the high pressure during the mechanical processing of cellulose, may damage the crystals' structure, resulting in nanosized cellulose fibers with reduced crystallinity (Wei et al. 2012; Xiang et al. 2016). In this work, the TEMPO oxidation time, the pressure and the passage numbers in the microfluidizer were optimal for the isolation of CNFs with relatively high crystallinity.

Thermal stability of raw and treated cellulosic fibers was investigated with TGA/DTG analysis. Figure 5a, b show the obtained TGA and DTG curves for all studied samples. From these results, the studied samples exhibited different degradation behaviors, depending on the applied treatment. The first degradation stage observed for all samples at 50–100 °C is due the evaporation of the absorbed moisture (Cao et al. 2012; Trache et al. 2014). The R-AF undergoes tow weight loss, the first one in the range 160–300 °C (with a maximum of 265 °C) due to hemicellulose and lignin degradation, and then the second one in the range of 300–400 °C (with a maximum of 337 °C) corresponds to the cellulose degradation (Kadem et al. 2018). AT-AF and CMF samples show only one degradation peak corresponding to degradation processes of cellulose, such as dehydration, decarboxylation, depolymerisation and decomposition of glycosyl units followed by the formation of a charred
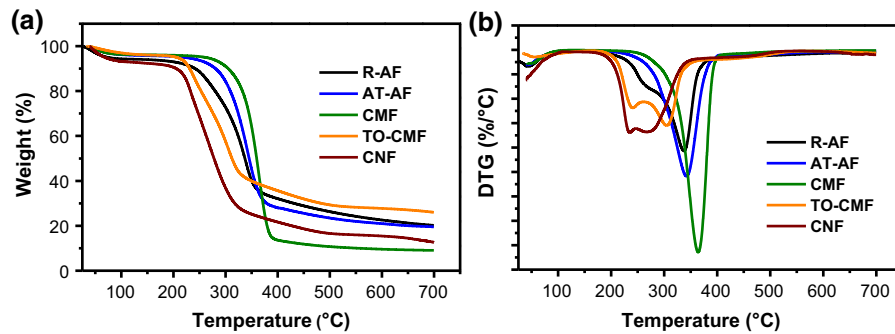
Fig. 5 **a** TGA and **b** DTG curves of R-AF, AT-AF, CMF, TO-CMF and CNF samples

residue (Trache et al. 2014). This finding indicates the effective removal of hemicelluloses and lignin, which makes the cellulose more exposed to thermal degradation (Kadem et al. 2018). Furthermore, the thermal degradation of R-AF, AT-AF and CMFs started at approximately 166 °C, 196 °C and 222 °C, respectively. While for the TO-CMF and CNF fibers, the degradation began at approximately 174 °C and 163 °C, respectively, and showed two peaks around 249 °C and 290 °C in DTG curves. The first degradation (peak at 249 °C) was primarily triggered by decarboxylation of sodium carboxylate groups introduced via TEMPO-mediated oxidation on the surface of TO-CMF and CNF fibers. While the second degradation was associated with the degradation of the main cellulose chains (Wu et al. 2019a). A minor difference was observed as a relatively lower thermal stability for CNFs, though the chemical compositions of TO-CMFs and CNFs are the same. The smaller dimensions of CNFs as compared to TO-CMFs can explain such differences in the thermal degradation of CNFs and TO-CMFs.

Nanocomposites processing and properties

PVA is a hydrophilic polymer exhibiting abundant hydroxyl groups, which makes it easy to process in water (El Achaby et al. 2018c). Furthermore, CNFs exhibit abundant carboxyl groups inserted on their surfaces, allowing potential intermolecular hydrogen bonding (Endo et al. 2013). The aqueous suspensions of PVA and CNFs were mixed in different compositions by varying the weight content of CNFs (from 0 to 15 wt%), and after water evaporation, transparent CNF-filled PVA nanocomposite films with thickness ranging from 75 to 80 μm were obtained.

FTIR analysis of nanocomposites

The chemical structure of the obtained nanocomposite films was examined using FTIR analysis (Fig. 6). It is worth noting that all characteristic IR bands typical of PVA polymer are presented in the spectrum of the produced pure PVA film (Tadokoro et al. 1956; Liu et al. 2013; Puangsin et al. 2017; Singh et al. 2018).The incorporation of CNFs into the PVA matrix induced small changes in the nanocomposites' spectra, which indicates the formation of interfacial interactions between CNFs and PVA components (Qua et al. 2009). In the spectra of nanocomposites, the intensity of the peak in the region of 1085 cm^{-1} (C–O
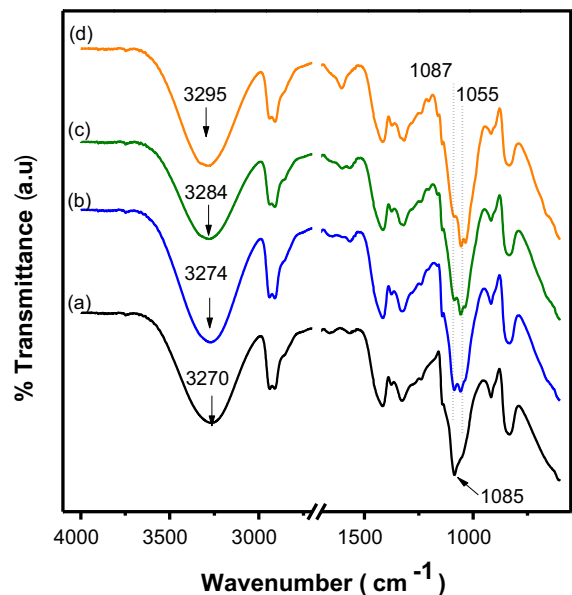

Fig. 6 FTIR spectra of PVA nanocomposite films at different CNF loadings: (a) neat PVA, (b) PVA-CNF-5, (c) PVA-CNF-10and (d) PVA-CNF-15

stretching in PVA) slightly increased after the addition of CNFs, due to the contribution of C–O stretching from the cellulosic component (CNF) (Qua et al. 2009). Remarkably, a slight shift of the OH peak (3274–3295 cm^{-1}) compared to pure PVA's OH peak (3270 cm^{-1}) was observed (Fig. 6). Additionally, the peak at 1085 cm^{-1} (C–O stretching) observed in neat PVA spectrum was split into two peaks at 1087 and 1055 cm^{-1} in nanocomposites' spectra, which correspond to the asymmetric ring breathing mode of cellulose and to the C–OH bending vibrations of alcohol groups present in cellulose, respectively (Abitbol et al. 2011; Fortunati et al. 2013). As a result, the shifting and splitting of –OH (3270 cm^{-1}) and C–O (1085 cm^{-1}) peaks are due to the interaction of hydroxyl groups of PVA with the carboxyl groups of the incorporated carboxy-functionalized CNFs (Liu et al. 2013).

Optical transmittance of nanocomposites

Figure 7 shows the UV–vis transmittance of the produced neat PVA and CNF-filled PVA nanocomposite films. It is well known that PVA is a transparent polymer (El Achaby et al. 2018c), and this was confirmed by the high transmittance (91% at 650 nm) determined in the visible light region (Fig. 7). However, the transmittance of neat PVA polymer was slightly decreased with increasing of CNF loading from 5 to 15 wt%. The transmittance of nanocomposite films reached 88%, 82% and 76% at 650 nm for PVA-CNF-5, PVA-CNF-10 and PVA-CNF-15, respectively, indicating that the optical transmittance level of PVA film was not largely affected by the
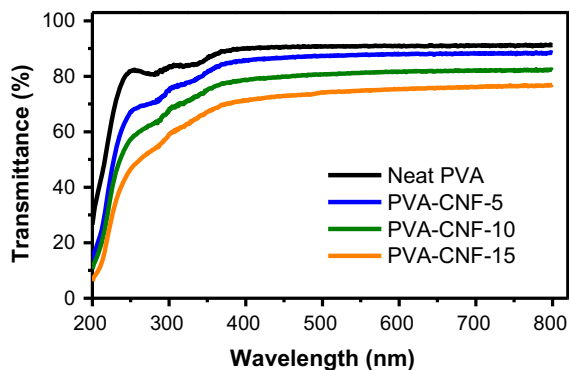

Fig. 7 UV–visible transmittance spectra of PVA nanocomposite films at different CNF loadings (0, 5, 10 and 15 wt%)

addition of CNFs. This is a good indication on the fine dispersion of CNFs within PVA polymer, resulting in structured nanocomposite films with high optical transmittance level (Kassab et al. 2019a).

Thermal properties of nanocomposites

The thermal stability of the prepared neat PVA and PVA-CNF nanocomposite films was investigated by TGA/DTG analysis. The obtained TGA and DTG curves are represented in Fig. 8a, b. The thermal parameters such as $T_{10\%}$, T_{max} and the residual char values at 700 °C are reported in Table 1. All samples undergo the same thermal degradation pattern and exhibited mainly three distinct steps. The first weight loss at 70–200 °C is likely caused by the evaporation of weak chemically and physically bonded water found in neat PVA and PVA-CNF nanocomposite films (Liu et al. 2013). While, the second weight loss at 200–400 °C can be attributed to the decomposition of the side chain of PVA (dehydration reaction), the beginning of CNF degradation and the formation of volatile products (Liu et al. 2013). Finally, a weight loss was observed at 400–550 °C corresponding to the decomposition of main chain of PVA.

It is worth noting that the $T_{10\%}$ decreased by increasing the CNF content (Table 1). This trend could be attributed to the low thermal degradation temperature of CNFs, which started to occur at approximately 200 °C (Fig. 5). However, the T_{max} of neat PVA and its nanocomposites with CNFs (5–15 wt%) was determined at 284, 292, 288 and 298 °C, respectively, indicating that the T_{max} increased with the addition of CNFs into PVA polymer. This finding is due the interfacial interaction between the PVA macromolecular chains with functionalized surface of CNF fillers, resulting in the restriction of the polymer chains mobility at the PVA-CNF interfaces (El Achaby et al. 2016) improving, in turn, the thermal degradation behavior of the resulted PVA-CNF nanocomposite films. At the end of each degradation test, solid char residue remains. The yield of this residual solid shifted to higher values after the addition of CNFs, especially for 10 and 15 wt% CNF loadings. It has been reported that the addition of nanoparticles would increase the char yield of polymers at high temperatures (Hamou et al. 2018).

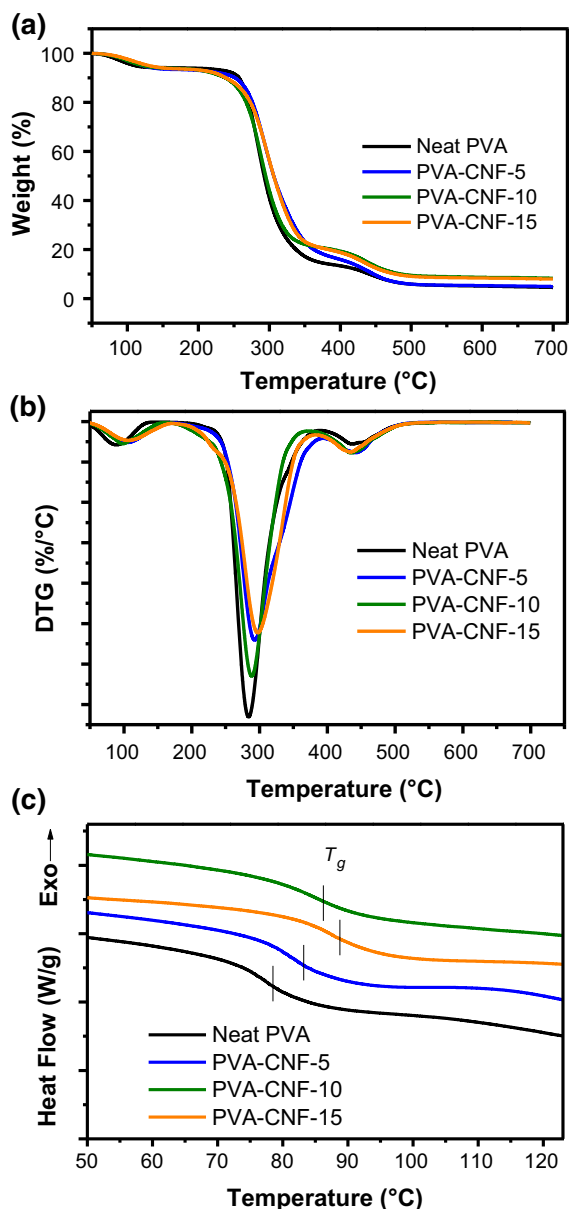The effect of CNF loadings on glass transition temperature (T_g) of the obtained nanocomposite films

Fig. 8 a TGA, **b** DTG and **c** DSC curves of PVA nanocomposite films at different CNF loadings (0, 5, 10 and 15 wt%)

was studied using DSC analysis, and the obtained curves of the first heating are presented in Fig. 8c, and the values of the T_g of all PVA-CNF nanocomposite films are summarized in Table 1. From these results, obviously, the T_g value was shifted to higher temperatures with the increase of CNF loadings as compared to neat PVA. The gradually increase of the T_g suggests the restriction of PVA macromolecular chain mobility, due to the strong intermolecular interaction between

the latter and the CNF (Endo et al. 2013; Puangsin et al. 2017). The created interactions induce an increase in the energy required for the T_g to occur (El Miri et al. 2015; Puangsin et al. 2017; Hamou et al. 2018).

Mechanical properties of nanocomposites

The mechanical properties of the prepared neat PVA and PVA-CNF nanocomposite films were characterized by uniaxial tensile tests. The measured tensile modulus and tensile strength are presented in Fig. 9. From the obtained results, it was found that the modulus and the strength were significantly increased with increasing the CNF content from 0 to 15 wt% (Fig. 9a, b). Indeed, when 5 wt% CNFs was added, the modulus and strength were increased by 25% and 33% compared to neat PVA, respectively.

Furthermore, the relatively high CNF content (15 wt%) resulted in a remarkable increase of the tensile modulus and strength with regard to neat PVA; an increase of 90 and 74% was observed for the modulus and strength when 15 wt% CNFs was added. This enhancement was attributed to the high aspect ratio and high crystallinity of the as-produced CNF nanofiller that can control PVA macromolecular chain movement during the deformation process (Cho and Park 2011; Guo et al. 2013; Puangsin et al. 2017). Furthermore, during the preparation of PVA-CNF nanocomposite films, strong hydrogen bonds could be formed between the functional groups presented on the surface of the CNFs (carboxyl and hydroxyl groups) and the hydroxyl groups in PVA chains (Wu et al. 2019c). These new bonds probably have replaced the original hydrogen bonds formed between the PVA chains, and hence strong nanofiber/matrix interface was developed (El Achaby et al. 2018d). Similar trend was reported for PVA-CNF nanocomposites (Li et al. 2014), where the mechanical properties increased with the increase of CNF content from 2 to 6 wt%; however, for CNF content greater than 6 wt%, the modulus and the tensile strength exhibited a declining trend, which was explained by the agglomeration phenomena of CNFs making the nanocomposites films more brittle (Li et al. 2014). The same trend was also reported in our previous work for CNC extracted from the same source (Alfa fibers), in which the incorporation of CNC up to 8 wt% showed improved tensile properties of various biopolymers such as alginate, *k*-

Table 1 The onset temperature ($T_{10\%}$), the maximum temperature (T_{max}), the residual weight percentage and the glass transition temperature (T_g) of PVA nanocomposite films at different CNF loadings (0, 5, 10 and 15 wt%)
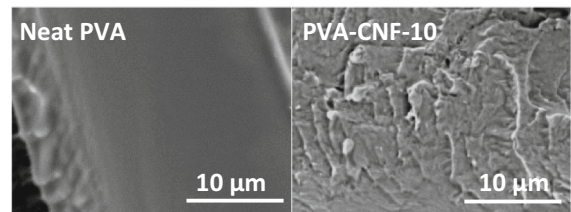
	$T_{10\%}$ (°C)	T_{max} (°C)	Residue at 700 °C (%)	T_g glass transition
Neat PVA	257	284	4.5	76
PVA-CNF-5	250	292	4.9	83
PVA-CNF-10	237	288	8.3	86
PVA-CNF-15	239	298	7.9	89
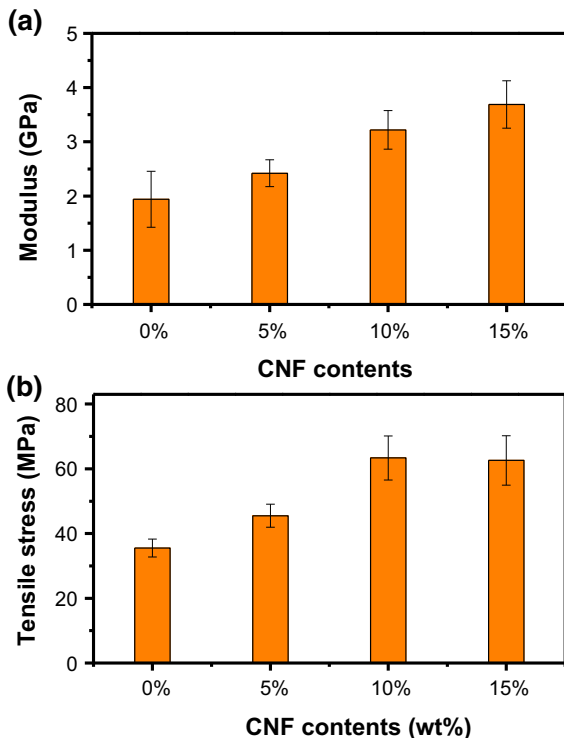
Fig. 9 a Tensile modulus and **b** tensile stress of PVA nanocomposite films at different CNF loadings (0, 5, 10 and 15 wt%)

Fig. 10 SEM images of the cryo-fractured cross-section of neat PVA film and PVA nanocomposite film containing 10 wt% CNF loading

This can be attributed primarily to the presence of strong interactions between CNF surfaces and PVA macromolecular chains (Endo et al. 2013), which is responsible for the improvement of the tensile properties of the produced nanocomposite films.

Conclusions

The successful extraction of carboxy-functionalized cellulose nanofibrils (CNFs) from Alfa fibers (*Stipa Tenacissima* plant) was achieved, demonstrating the opportunity for the potential use of these natural fibers that are largely abundant in many countries. The physico-chemical characterizations confirmed that the applied pre-treatments (alkali and bleaching) were suitable for the removal of non-cellulosic compounds, resulting in the production of pure micro-sized cellulose fibers. After subjecting the cellulose fibers to TEMPO-mediated oxidation followed by mechanical disintegration, carboxy-functionalized CNFs were isolated with diameter ranging from 1.4 to 4.6 nm and length of up to several microns. The as-produced CNFs exhibited a crystallinity of 89%, which is found to be very high compared to that obtained from other sources. The nanoreinforcement potential of the as-extracted CNFs was evaluated using PVA as

carrageenan and chitosan matrices (El Achaby et al. 2018d).

Morphology of nanocomposites

SEM micrographs of the cryo-fractured cross-section of neat PVA and its nanocomposite film containing 10 wt% CNFs are illustrated in Fig. 10. It is worth noting that the cross-section of the neat PVA film appears smooth and uniform, while an increase in section roughness was detected with the presence of CNFs.

polymeric matrix. Increases of 90% of tensile modulus and 74% of tensile strength was observed for PVA nanocomposite containing 15 wt% CNFs, respectively. The optical transmittance was reduced from 91% (at 650 nm) for neat PVA polymer to 88%, 82% and 76% for PVA nanocomposites containing 5, 10 and 15 wt% CNFs, respectively. The addition of CNFs also increased the glass transition temperature from 76 °C for neat PVA to 89 °C for PVA nanocomposite containing 15 wt%. The obtained results indicated that the extracted CNFs exhibit a high ability to reinforce PVA polymer. Consequently, Alfa plant, which is a fast-growing perennial plant, cellulose-rich, inexpensive and renewable, has been proposed as a viable source for cellulose nanofibrils production. Besides, the extracted CNFs from Alfa fibers, with excellent properties, can be considered as a potential candidate to produce nanostructured polymer nanocomposites with enhanced properties.

References

Abitbol T, Johnstone T, Quinn TM, Gray DG (2011) Reinforcement with cellulose nanocrystals of poly(vinyl alcohol) hydrogels prepared by cyclic freezing and thawing. Soft Matter 7:2373–2379. https://doi.org/10.1039/c0sm01172j

Belouadah Z, Ati A, Rokbi M (2015) Characterization of new natural cellulosic fiber from Lygeum spartum L. Carbohydr Polym 134:429–437. https://doi.org/10.1016/j.carbpol.2015.08.024

Borchani KE, Carrot C, Jaziri M (2015) Untreated and alkali treated fibers from Alfa stem: effect of alkali treatment on structural, morphological and thermal features. Cellulose 22:1577–1589. https://doi.org/10.1007/s10570-015-0583-5

Boufi S, Kaddami H, Dufresne A (2014) Mechanical performance and transparency of nanocellulose reinforced polymer nanocomposites. Macromol Mater Eng 299:560–568. https://doi.org/10.1002/mame.201300232

Brinchi L, Cotana F, Fortunati E, Kenny JM (2013) Production of nanocrystalline cellulose from lignocellulosic biomass: technology and applications. Carbohydr Polym 94:154–169

Cao X, Ding B, Yu J, Al-Deyab SS (2012) Cellulose nanowhiskers extracted from TEMPO-oxidized jute fibers. Carbohydr Polym 90:1075–1080. https://doi.org/10.1016/j.carbpol.2012.06.046

Chen YW, Lee HV, Abd Hamid SB (2017) Facile production of nanostructured cellulose from *Elaeis guineensis* empty fruit bunch via one pot oxidative-hydrolysis isolation approach. Carbohydr Polym 157:1511–1524. https://doi.org/10.1016/j.carbpol.2016.11.030

Cho MJ, Park BD (2011) Tensile and thermal properties of nanocellulose-reinforced poly(vinyl alcohol) nanocomposites. J Ind Eng Chem 17:36–40. https://doi.org/10.1016/j.jiec.2010.10.006

Collazo-Bigliardi S, Ortega-Toro R, Chiralt Boix A (2018) Isolation and characterisation of microcrystalline cellulose and cellulose nanocrystals from coffee husk and comparative study with rice husk. Carbohydr Polym 191:205–215. https://doi.org/10.1016/j.carbpol.2018.03.022

Curvello R, Raghuwanshi VS, Garnier G (2019) Engineering nanocellulose hydrogels for biomedical applications. Adv Colloid Interface Sci 267:47–61. https://doi.org/10.1016/J.CIS.2019.03.002

Dong H, Sliozberg YR, Snyder JF et al (2015) Highly transparent and toughened poly(methyl methacrylate) nanocomposite films containing networks of cellulose nanofibrils. ACS Appl Mater Interfaces 7:25464–25472. https://doi.org/10.1021/acsami.5b08317

El Achaby M, El Miri N, Snik A et al (2016) Mechanically strong nanocomposite films based on highly filled carboxymethyl cellulose with graphene oxide. J Appl Polym Sci 133:1–11. https://doi.org/10.1002/app.42356

El Achaby M, El Miri N, Hannache H et al (2018a) Cellulose nanocrystals from Miscanthus fibers: insights into rheological, physico-chemical properties and polymer reinforcing ability. Cellulose 25:6603–6619. https://doi.org/10.1007/s10570-018-2047-1

El Achaby M, El Miri N, Hannache H et al (2018b) Production of cellulose nanocrystals from vine shoots and their use for the development of nanocomposite materials. Int J Biol Macromol 117:592–600. https://doi.org/10.1016/j.ijbiomac.2018.05.201

El Achaby M, Kassab Z, Aboulkas A et al (2018c) Reuse of red algae waste for the production of cellulose nanocrystals and its application in polymer nanocomposites. Int J Biol Macromol 106:681–691. https://doi.org/10.1016/j.ijbiomac.2017.08.067

El Achaby M, Kassab Z, Barakat A, Aboulkas A (2018d) Alfa fibers as viable sustainable source for cellulose nanocrystals extraction: application for improving the tensile properties of biopolymer nanocomposite films. Ind Crops Prod 112:499–510. https://doi.org/10.1016/j.indcrop.2017.12.049

El Miri N, Abdelouahdi K, Zahouily M et al (2015) Bionanocomposite films based on cellulose nanocrystals filled polyvinyl alcohol/chitosan polymer blend. J Appl Polym Sci 132:1–13. https://doi.org/10.1002/app.42004

Endo R, Saito T, Isogai A (2013) TEMPO-oxidized cellulose nanofibril/poly(vinyl alcohol) composite drawn fibers. Polymer (Guildf) 54:935–941. https://doi.org/10.1016/j.polymer.2012.12.035

Ferrer A, Pal L, Hubbe M (2017) Nanocellulose in packaging: advances in barrier layer technologies. Ind Crops Prod 95:574–582. https://doi.org/10.1016/j.indcrop.2016.11.012

Fortunati E, Puglia D, Luzi F et al (2013) Binary PVA bio-nanocomposites containing cellulose nanocrystals extracted from different natural sources: part I. Carbohydr Polym 97:825–836. https://doi.org/10.1016/j.carbpol.2013.03.075

French AD (2014) Idealized powder diffraction patterns for cellulose polymorphs. Cellulose 21:885–896. https://doi.org/10.1007/s10570-013-0030-4

French AD, Santiago Cintrón M (2013) Cellulose polymorphy, crystallite size, and the Segal Crystallinity Index. Cellulose 20:583–588. https://doi.org/10.1007/s10570-012-9833-y

Gazzotti S, Rampazzo R, Hakkarainen M et al (2019) Cellulose nanofibrils as reinforcing agents for PLA-based nanocomposites: an in situ approach. Compos Sci Technol 171:94–102. https://doi.org/10.1016/j.compscitech.2018.12.015

Goetz LA, Naseri N, Nair SS et al (2018) All cellulose electrospun water purification membranes nanotextured using cellulose nanocrystals. Cellulose 25:3011–3023. https://doi.org/10.1007/s10570-018-1751-1

Guo C, Zhou L, Lv J (2013) Effects of expandable graphite and modified ammonium polyphosphate on the flame-retardant and mechanical properties of wood flour-polypropylene composites. Polym Polym Compos 21:449–456. https://doi.org/10.1177/096739111302100706

Hamou KB, Kaddami H, Dufresne A et al (2018) Impact of TEMPO-oxidization strength on the properties of cellulose nanofibril reinforced polyvinyl acetate nanocomposites. Carbohydr Polym 181:1061–1070. https://doi.org/10.1016/j.carbpol.2017.11.043

Jose J, Thomas V, Vinod V et al (2019) Nanocellulose based functional materials for supercapacitor applications. J Sci Adv Mater Devices. https://doi.org/10.1016/j.jsamd.2019.06.003

Joy J, Jose C, Yu X et al (2017) The influence of nanocellulosic fiber, extracted from Helicteres isora, on thermal, wetting and viscoelastic properties of poly(butylene succinate) composites. Cellulose 24:4313–4323. https://doi.org/10.1007/s10570-017-1439-y

Kadem S, Irinislimane R, Belhaneche-Bensemra N (2018) Novel biocomposites based on sunflower oil and alfa fibers as renewable resources. J Polym Environ 26:3086–3096. https://doi.org/10.1007/s10924-018-1196-5

Kassab Z, Aziz F, Hannache H et al (2019a) Improved mechanical properties of k-carrageenan-based nanocomposite films reinforced with cellulose nanocrystals. Int J Biol Macromol 123:1248–1256. https://doi.org/10.1016/j.ijbiomac.2018.12.030

Kassab Z, El Achaby M, Tamraoui Y et al (2019b) Sunflower oil cake-derived cellulose nanocrystals: extraction, physico-chemical characteristics and potential application. Int J Biol Macromol 136:241–252. https://doi.org/10.1016/j.ijbiomac.2019.06.049

Kılınç AÇ, Köktaş S, Seki Y et al (2018) Extraction and investigation of lightweight and porous natural fiber from Conium maculatum as a potential reinforcement for composite materials in transportation. Compos Part B Eng 140:1–8. https://doi.org/10.1016/j.compositesb.2017.11.059

Koga H, Saito T, Kitaoka T et al (2013) Transparent, conductive, and printable composites consisting of TEMPO-oxidized nanocellulose and carbon nanotube. Biomacromolecules 14:1160–1165. https://doi.org/10.1021/bm400075f

Kumar A, Negi YS, Choudhary V, Bhardwaj NK (2014) Characterization of cellulose nanocrystals produced by acid-hydrolysis from sugarcane bagasse as agro-waste. J Mater Phys Chem 2:1–8. https://doi.org/10.12691/jmpc-2-1-1

Lam NT, Chollakup R, Smitthipong W et al (2017) Characterization of cellulose nanocrystals extracted from sugarcane bagasse for potential biomedical materials. Sugar Tech 19:539–552. https://doi.org/10.1007/s12355-016-0507-1

Lasseuguette E (2008) Grafting onto microfibrils of native cellulose. Cellulose 15:571–580. https://doi.org/10.1007/s10570-008-9200-1

Li W, Wu Q, Zhao X et al (2014) Enhanced thermal and mechanical properties of PVA composites formed with filamentous nanocellulose fibrils. Carbohydr Polym 113:403–410. https://doi.org/10.1016/j.carbpol.2014.07.031

Liu D, Sun X, Tian H et al (2013) Effects of cellulose nanofibrils on the structure and properties on PVA nanocomposites. Cellulose 20:2981–2989. https://doi.org/10.1007/s10570-013-0073-6

Liu D, Bian Q, Li Y et al (2016) Effect of oxidation degrees of graphene oxide on the structure and properties of poly (vinyl alcohol) composite films. Compos Sci Technol 129:146–152. https://doi.org/10.1016/j.compscitech.2016.04.004

Mabrouk AB, Kaddami H, Boufi S et al (2012) Cellulosic nanoparticles from alfa fibers (Stipa tenacissima): extraction procedures and reinforcement potential in polymer nanocomposites. Cellulose 19:843–853. https://doi.org/10.1007/s10570-012-9662-z

Mandal A, Chakrabarty D (2011) Isolation of nanocellulose from waste sugarcane bagasse (SCB) and its characterization. Carbohydr Polym 86:1291–1299. https://doi.org/10.1016/j.carbpol.2011.06.030

Panyasiri P, Yingkamhaeng N, Lam NT, Sukyai P (2018) Extraction of cellulose nanofibrils from amylase-treated cassava bagasse using high-pressure homogenization. Cellulose 25:1757–1768. https://doi.org/10.1007/s10570-018-1686-6

Poyraz B, Tozluoğlu A, Candan Z et al (2017) Influence of PVA and silica on chemical, thermo-mechanical and electrical properties of Celluclast-treated nanofibrillated cellulose composites. Int J Biol Macromol 104:384–392. https://doi.org/10.1016/j.ijbiomac.2017.06.018

Puangsin B, Soeta H, Saito T, Isogai A (2017) Characterization of cellulose nanofibrils prepared by direct TEMPO-mediated oxidation of hemp bast. Cellulose 24:3767–3775. https://doi.org/10.1007/s10570-017-1390-y

Qua EH, Hornsby PR, Sharma HSS et al (2009) Preparation and characterization of Poly(vinyl alcohol) nanocomposites made from cellulose nanofibers. J Appl Polym Sci 113:2238–2247. https://doi.org/10.1002/app.30116

Saito T, Kimura S, Nishiyama Y, Isogai A (2007) Cellulose nanofibers prepared by TEMPO-mediated oxidation of native cellulose. Biomacromolecules 8:2485–2491. https://doi.org/10.1021/bm0703970

Singh S, Gaikwad KK, Lee YS (2018) Antimicrobial and antioxidant properties of polyvinyl alcohol bio composite films containing seaweed extracted cellulose nano-crystal and basil leaves extract. Int J Biol Macromol 107:1879–1887. https://doi.org/10.1016/j.ijbiomac.2017.10.057

Tadokoro H, Seki S, Nitta I (1956) Some information on the infrared absorption spectrum of poly(vinyl alcohol) from deuteration and pleochroism. J Polym Sci 669:563–566. https://doi.org/10.1002/pol.1956.1202210227

Thomas B, Raj MC, Athira KB et al (2018) Nanocellulose, a versatile green platform: from biosources to materials and their applications. Chem Rev 118:11575–11625. https://doi.org/10.1021/acs.chemrev.7b00627

Trache D (2018) Nanocellulose as a promising sustainable material for biomedical applications. AIMS Mater Sci 5:201–205. https://doi.org/10.3934/matersci.2018.2.201

Trache D, Donnot A, Khimeche K et al (2014) Physico-chemical properties and thermal stability of microcrystalline cellulose isolated from Alfa fibres. Carbohydr Polym 104:223–230. https://doi.org/10.1016/j.carbpol.2014.01.058

Trache D, Hussin MH, Hui Chuin CT et al (2016a) Microcrystalline cellulose: isolation, characterization and bio-composites application—a review. Int J Biol Macromol 93:789–804. https://doi.org/10.1016/j.ijbiomac.2016.09.056

Trache D, Khimeche K, Mezroua A, Benziane M (2016b) Physicochemical properties of microcrystalline nitrocellulose from Alfa grass fibres and its thermal stability. J Therm Anal Calorim 124:1485–1496. https://doi.org/10.1007/s10973-016-5293-1

Trache D, Hussin MH, Haafiz MKM, Thakur VK (2017) Recent progress in cellulose nanocrystals: sources and production. Nanoscale 9:1763–1786. https://doi.org/10.1039/c6nr09494e

Wang Z, Qiao X, Sun K (2018) Rice straw cellulose nanofibrils reinforced poly(vinyl alcohol) composite films. Carbohydr Polym 197:442–450. https://doi.org/10.1016/j.carbpol.2018.06.025

Wei Q, Tao D, Xu Y (2012) Nanofibers: principles and manufacture. Funct Nanofibers Their Appl. https://doi.org/10.1533/9780857095640.1.1

Wu J, Du X, Yin Z et al (2019a) Preparation and characterization of cellulose nanofibrils from coconut coir fibers and their reinforcements in biodegradable composite films. Carbohydr Polym 211:49–56. https://doi.org/10.1016/j.carbpol.2019.01.093

Wu T, Cai B, Wang J et al (2019b) TEMPO-oxidized cellulose nanofibril/layered double hydroxide nanocomposite films with improved hydrophobicity, flame retardancy and mechanical properties. Compos Sci Technol 171:111–117. https://doi.org/10.1016/j.compscitech.2018.12.019

Wu Y, Tang Q, Yang F et al (2019c) Mechanical and thermal properties of rice straw cellulose nanofibrils-enhanced polyvinyl alcohol films using freezing-and-thawing cycle method. Cellulose 26:3193–3204. https://doi.org/10.1007/s10570-019-02310-6

Xiang Z, Gao W, Chen L et al (2016) A comparison of cellulose nanofibrils produced from *Cladophora glomerata* algae and bleached eucalyptus pulp. Cellulose 23:493–503. https://doi.org/10.1007/s10570-015-0840-7

Zhao Y, Moser C, Lindström ME et al (2017) Cellulose nanofibers from softwood, hardwood, and tunicate: preparation-structure-film performance interrelation. ACS Appl Mater Interfaces 9:13508–13519. https://doi.org/10.1021/acsami.7b01738